High-Efficiency Operation of Membrane Distributed-Reflector Lasers on Silicon Substrate

Takuo Hiratani, *Student Member, IEEE*, Daisuke Inoue, *Student Member, IEEE*, Takahiro Tomiyasu, Kai Fukuda,
Tomohiro Amemiya, *Member, IEEE*, Nobuhiko Nishiyama, *Senior Member, IEEE*,
and Shigehisa Arai, *Fellow, IEEE*

Abstract—To advance on-chip optical interconnections, membrane distributed-reflector (DR) lasers with low threshold current and high-efficiency operation at one side output were realized. First, a membrane distributed Bragg reflector (DBR) laser with 80-μm-long active section and 50-μm-long DBR section was fabricated to clarify the DBR reflectivity. An external differential quantum efficiency of 35% for the output from the front facet was obtained, and the DBR reflectivity was estimated to be 75%. Next, a membrane DR laser with 61-μm-long distributed feedback section and 50-μm-long DBR section was fabricated. A threshold current of 0.48 mA, external differential quantum efficiency from the front side waveguide of 26%, and light output ratio from the front to the rear sides of 13 were obtained. The lasing spectrum showed a single-mode operation with a side-mode suppression-ratio (SMSR) of 40 dB. Finally, small-signal direct modulation was carried out and a modulation current efficiency factor of 7.9 GHz/mA$^{1/2}$ and 7 GHz/mA$^{1/2}$ were, respectively, obtained for the 30-μm-long and 61-μm-long devices.

Index Terms—Membrane laser, distributed-reflector laser, semiconductor laser, optical interconnects.

I. INTRODUCTION

THE performance of large scale integrated (LSI) circuits has dramatically improved since the scaling law was proposed in 1974 [1]. However, in recent years, issues such as signal delay and Joule heating have become problematic [2], [3], and threaten the future progress of LSI. In order to overcome these problems, replacement of the electrical global interconnects with optical interconnects has been proposed and widely studied [4]–[6]. In the case of optical interconnects on LSI, the available energy cost to send one-bit signal in the system is estimated to be

T. Hiratani, D. Inoue, T. Tomiyasu, and K. Fukuda are with the Department of Electrical and Electronic Engineering, Tokyo Institute of Technology, Tokyo 152-8552, Japan (e-mail: hiratani.t.aa@m.titech.ac.jp; inoue.d.ac@m.titech.ac.jp; tomiyasu.t.aa@m.titech.ac.jp; fukuda.k.an@m.titech.ac.jp).

T. Amemiya, N. Nishiyama, and S. Arai are with the Institute of Innovative Research, Tokyo Institute of Technology, Tokyo 152-8552, Japan (e-mail: amemiya.t.ab@m.titech.ac.jp; nishiyama@ee.e.titech.ac.jp; arai@pe.titech.ac.jp).

Color versions of one or more of the figures in this paper are available online at http://ieeexplore.ieee.org.

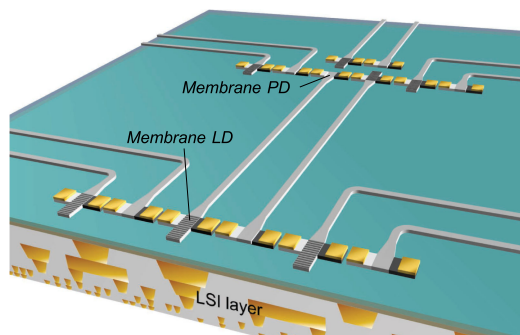Digital Object Identifier 10.1109/JSTQE.2017.2704289

Fig. 1. Schematic image of membrane photonic integrated circuits on LSI.

less than 100 fJ/bit [7]. Therefore, a light source with ultra-low power consumption is necessary for the realization of on-chip optical interconnects.

In terms of low-power-consumption operation, vertical-cavity surface-emitting lasers (VCSELs) [8]–[11], micro-disk lasers [12], [13], and photonic crystal lasers [14]–[17] were reported. Although VCSELs are suitable for low power consumption with sufficient light output power, 45°-tilted micro-mirrors are required for in-plane integration [18]. While micro-disk lasers and photonic crystal lasers are very attractive for ultra-low threshold current operation due to their strong optical confinement effect into a very small active region, very strong optical confinement leads to lower optical output power. In the optical interconnects, the required optical power level at the receiver side is in the order of several tens μW for signal speeds faster than 10 Gbit/s with bit-error-rates (BER) lower than 10^{-9}.

We proposed and demonstrated membrane distributed feedback (DFB) lasers as well as membrane distributed-reflector (DR) lasers as light sources with low power consumption operation [19]–[22] for membrane photonic integrated circuits (MPICs) on Si as shown in Fig. 1. Because the membrane structure consists of a thin semiconductor core layer sandwiched by low refractive-index cladding layers, similar to high-index-contrast waveguides, the optical confinement factor of the active region is approximately three times higher than that of conventional in-plane semiconductor lasers. Therefore, it leads to not only an enhancement of the optical modal gain but also that of index-coupling coefficient of the grating structure,

and these will result in extremely low threshold current operation without sacrificing the differential quantum efficiency. In MPICs, III-V materials are used for both active and passive devices. The use of a III–V active layer on a Si-based passive waveguide was reported as another approach to form the photonic integrated circuits on Si substrates. Although the differential quantum efficiency was quite low due to difficulty in coupling to the Si waveguide in initial devices [23], DFB type lasers on Si substrate with improved light output characteristics and low threshold current of around 10 mA were realized [24], [25]. Furthermore, high-speed modulation up to 40 Gbit/s was realized for integrated InP/SOI DFB lasers [26]. However, the operating energy was estimated to be a few pJ/bit, which seems to be much higher than that required for on-chip optical interconnection. Although these devices are suitable for wavelength division multiplexing (WDM) systems for short-reach communication inside data centers, it is difficult to apply for on-chip optical interconnections in terms of operating energy. Another design to reduce the active region volume is required for low energy operation.

After the first room-temperature continuous-wave (RT-CW) operation of a membrane DFB laser under optical pumping in 2001 [27], various current-injection-type membrane lasers such as membrane DFB lasers directly bonded on an SOI substrate [28]–[30] were reported. RT-CW operation of membrane-type Fabry-Perot (FP) lasers grown on semi-insulating (SI) InP substrate was achieved with a threshold current of 11 mA for a cavity length of 720 μm, where an external differential quantum efficiency (DQE: η_d) of 33% was obtained while the internal quantum efficiency (IQE: η_i) was estimated to be only 40% [31] by using the lateral current injection (LCI) structure [32]. Then IQE was improved to 70% (DQE of 59%) for a similar cavity size by increasing the separation between quantum-wells for better carrier injection in the LCI structure [33]. As for the fabrication of the membrane DFB cavity structure, surface grating structures on an additional a-Si top layer [34], [35] or InP top layer [36], [37] were reported, however the threshold current was in the order of 10 mA or so under a pulsed condition.

RT-CW operation of a membrane FP laser bonded on Si substrate was demonstrated [38], with a threshold current of 2.5 mA (cavity length of 350 μm and the stripe width of 0.7 μm) and IQE of 75% by reduction of thermal resistance. Then RT-CW operation of membrane DFB lasers were demonstrated and the threshold current was reduced to 0.39 mA and 0.23 mA by adopting a narrow stripe (0.2 μm) geometry [39] and by a short cavity (50 μm) structure [40], respectively. Integration of the membrane DFB laser with a p-i-n-photodiode (PIN-PD) was also demonstrated [41]. Recently, high-speed direct modulation characteristics of a membrane DFB laser with a modulation current efficiency of 9.9 GHz/mA$^{1/2}$ were reported [42], and low bias current 10 Gb/s data transmission with a bit-error-rate (BER) of 1×10^{-9} was achieved using an optical amplifier [43].

However, these devices have poor light output characteristics. The DR structure, which improves the light output efficiency [44]–[47], was introduced, and an asymmetric light output characteristic with the ratio from the front to the rear sides of 6.7 was achieved [48]. Energy cost analysis of the membrane DR lasers was also carried out, and a suitable cavity structure was pro-
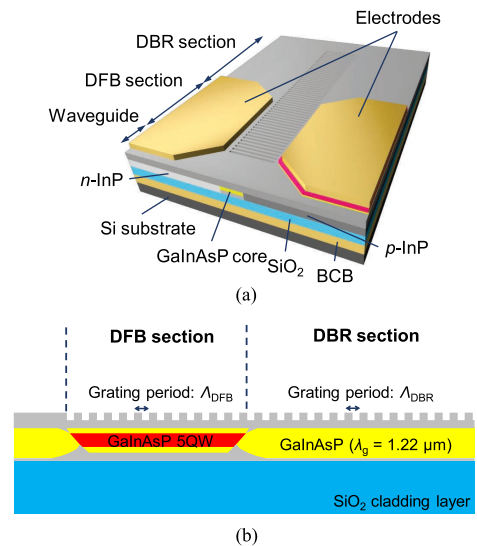

Fig. 2. (a) Schematic structure and (b) cross section of membrane DR laser.

posed in terms of the energy cost [49]. Furthermore, although a membrane DR laser integrated with a spot size converter for data center use was reported [50], [51], further reduction of threshold current is required for on-chip light sources.

In this paper, the characteristics of membrane DR lasers are shown in order to realize low threshold current and high efficiency operation. First, the design of the membrane DR laser is shown in Section II. Next, static characteristics of membrane DR lasers are shown in Section III. The characteristics of membrane distributed-Bragg-reflector (DBR) lasers are also shown in order to estimate the reflectivity of the DBR formed in the membrane structure. In Section IV, direct modulation characteristics, the bias current dependence of a small signal response, as well as 10 Gbit/s large signal modulation, of the membrane DR laser are presented.

II. DESIGN AND FABRICATION

In this section, the design of membrane DR laser and the fabrication process are shown. Fig. 2 shows a schematic structure and its cross section along the cavity direction of a membrane DR laser which has a DFB section with an active layer, a DBR section with surface grating structure on the passive waveguide, and passive waveguides connected to the back and front of the laser. In the membrane structure, a lateral current injection (LCI) structure with a lateral *pin* junction was adopted. This DR structure realizes high reflectivity for the lasing wavelength by setting the periods of DFB section and DBR section properly. We set the DFB period to match the shorter wavelength side mode of the stop band of the DFB section to the center wavelength (the Bragg wavelength) of the DBR section. The reflectivity of the DBR was designed to be higher than 95% for the DBR section longer than 90 μm [48]. In this calculation, the waveguide loss of the passive section was assumed to be 12 cm^{-1} including the material absorption loss.

Here, the energy cost for data transmission under the conditions of 10 Gb/s operation, corresponding to a 3 dB bandwidth of 7.7 GHz, and a light output power of 0.16 mW, which is
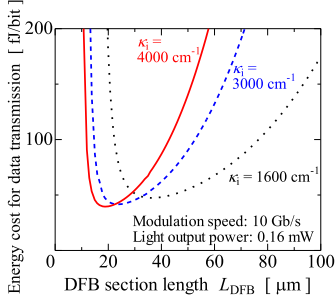
Fig. 3. Energy cost for data transmission as a function of DFB section length for various index-coupling coefficients κ_i.
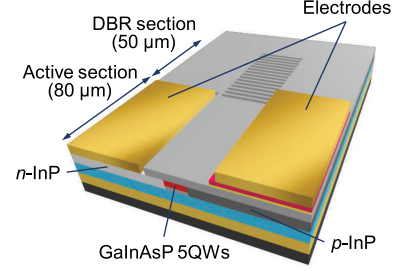

Fig. 4. Schematic structure of fabricated membrane DBR laser.

Fig. 5. Current-light output and current-voltage characteristics of membrane DBR laser.

required for on-chip light sources [22], [49], was estimated for various index-coupling coefficients κ_i as shown in Fig. 3. We did not treat the thermal properties, as investigated in our previous work [52]. The calculation was carried out for a stripe width of 1 μm and a DBR section length of 100 μm by using the transfer matrix method (TMM) [53], where the IQE and waveguide loss of the DFB section were assumed to be 75% and 21 cm^{-1}, respectively. The reflection loss between the DFB section and the DBR section was neglected because a reflection of -42 dB was estimated by the finite difference method (FDM) and the eigen-mode expansion method (EME) calculation [54]. In order to estimate the operating energy, it was assumed that the resistance of the p-InP is dominant. The p-InP resistivity of 0.035 $\Omega\cdot$cm and a distance between the p-electrode and active region of 1.2 μm were used [49]. The result shows that the low energy cost operation of less than 100 fJ/bit can be expected for the short cavity structure with a DFB section length of less than 50 μm. Furthermore, it is possible to reduce the energy cost by using a shorter cavity structure with a higher index-coupling coefficient κ_i. In the case of $\kappa_i = 4000$ cm^{-1}, the energy cost (at 10 Gbit/s and 0.16 mW output) can be reduced to 40 fJ/bit with a DFB section length of 19 μm.

Next, the fabrication process is briefly explained. The initial wafer structure was almost the same as that used in previous work [48]. The difference was the doping concentration of the p-InP upper cladding layer which was reduced to 5×10^{17} cm^{-3} in order to reduce the waveguide loss, and p^+-GaInAs (100 nm) and p^+-GaInAsP (20 nm) were used for better contact resistance. The etch stop layers and the 270-nm-thick core layer including strain-compensated GaInAsP five quantum-wells (5QWs) were grown on n-InP substrate by gas-source molecular-beam-epitaxy (GS-MBE). The process contains formation of the laser structure, benzocyclobutene (BCB) bonding, evaporation of electrodes, and formation of the surface grating. In the formation of the laser structure, a GaInAsP passive waveguide layer was selectively regrown and a *pin* junction was formed by two step selective regrowths of n-InP and p-InP. Next, 1-μm-thick SiO$_2$ cladding was deposited, and the laser wafer was bonded up-side down on a Si substrate by BCB bonding. After the bonding, the membrane structure was obtained by removing the InP substrate side and etch stop layers, and the contact layer was formed, where Au/Zn/Au/Ti/Au (25 nm/50 nm/300 nm/25 nm/250 nm) for the p-electrode and
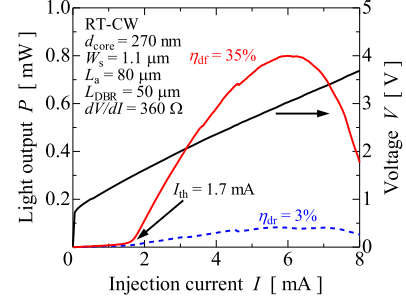
Ti/Au (25 nm/250 nm) for the n-electrode were evaporated. The p-electrode was annealed at 370 °C for 1 m. Finally, the surface gratings at both DFB and DBR sections were formed by electron beam lithography and wet chemical etching by using a solution of HCl:CH$_3$COOH:H$_2$O$_2$:H$_2$O = 2:20:1:30 at 10 °C for 2 s.

III. STATIC CHARACTERISTICS

First, the membrane DBR laser was fabricated for the estimation of the reflectivity of the DBR. The schematic structure of the fabricated membrane DBR laser used for this measurement is shown in Fig. 4. The surface grating was formed at only the DBR section, and the front facet was formed by cleaving at the active section. A device with stripe width of 1.1 μm, active section length of 80 μm, and DBR section length of 50 μm was used for evaluation of the light output characteristics. Fig. 5 shows the current-light output and current-voltage characteristics, where a threshold current of 1.7 mA, external differential quantum efficiency (DQE) from the front facet η_{df} and rear facet η_{dr} of 35% and 3%, respectively, and maximum light output of 0.8 mW were obtained thanks to the introduction of the rear DBR. A threshold voltage V_{th} of 1.4 V and differential resistance dV/dI of 360 Ω were obtained.

The DBR reflectivity R_{DBR} has the relation

$$\frac{P_f}{P_r} = \frac{\eta_{df}}{\eta_{dr}} = \frac{1 - R_f}{1 - R_{DBR}} \sqrt{\frac{R_{DBR}}{R_f}}, \qquad (1)$$

where P_f/P_r is the light output ratio and R_f is the reflectivity at the front facet [55]. Estimation of the actual external differential quantum efficiency from the rear DBR of η'_{dr} is required because the fabricated device has a 370-μm-long waveguide backside of the DBR. The external differential quantum efficiency from the rear DBR is expressed by $\eta'_{dr} = \eta_{dr} \cdot e^{\alpha L}/(1 - R_r) = 6\%$.

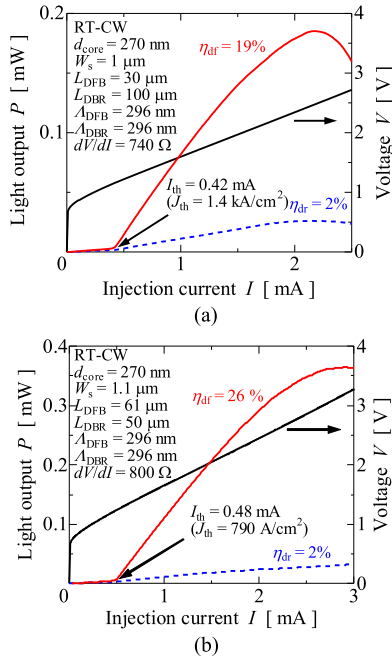Fig. 6. Current-light output and current-voltage characteristics of membrane DR lasers with (a) 30-μm-long DFB section and 100-μm-long DBR section and (b) 61-μm-long DFB section and 50-μm-long DBR section.

Fig. 7. Power conversion efficiency of the membrane DR laser.

Fig. 8. Lasing spectrum of membrane DR laser at bias current of 2.88 mA.

Here, an R_r of 22% and waveguide loss of $12\,cm^{-1}$ was assumed. Therefore, the reflectivity of the DBR was estimated to be 75% by using (1). From the theoretical analysis, the reflectivity of the DBR with a DBR length of 50 μm was estimated to be 98%. The difference between these values can be attributed to a scattering loss at the surface grating.

Next, membrane DR lasers with DFB section lengths of 30 μm and 61 μm were fabricated. Fig. 6(a) shows the current-light output and current-voltage characteristics of the fabricated device with a stripe width of 1 μm, and a grating period of 296 nm for both the DFB and DBR sections. This design comes from a slightly lower refractive index of the DBR section compared with that of the DFB section. For the measurement, the facets were formed by cleaving the waveguide section to create the front and rear facets without any coating. For stable single mode operation, anti-reflection coating is required in order to suppress the effect of facet phase and Fabry-Perot resonance between the cleaved facet and front side of the DFB section. However, the reflection can be suppressed by the taper structure between the laser and waveguide on MPICs. The length of the front waveguide was 60 μm. A threshold current of 0.42 mA (corresponding threshold current density of $1.4\,kA/cm^2$), external differential quantum efficiency from front facet and rear facet, η_{df} and η_{dr}, of 19% and 2%, light output ratio of 9.5, and maximum light output power of 0.19 mW were obtained. Furthermore, a threshold voltage V_{th} of 1.1 V and differential resistance dV/dI of 740 Ω were obtained. The reason for low voltage operation is the reduction of contact resistance and sheet resistance thanks to the diffusion of Zn to the p-InP layer by the introduction of the Au/Zn/Au electrode. Next, the fab-
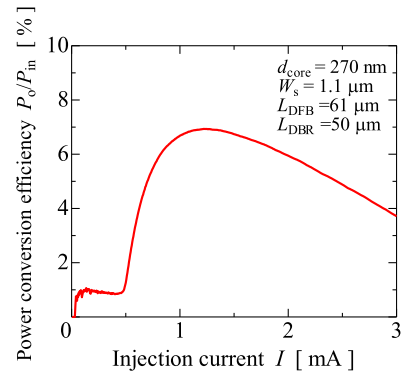
ricated membrane DR laser with 61-μm-long DFB section and 50-μm-long DBR section was measured, as shown in Fig. 6(b), where a threshold current of 0.48 mA (corresponding threshold current density of $790\,A/cm^2$), η_{df} of 26%, and maximum light output power of 0.36 mW were obtained. This device has no front waveguide, which means the device is cleaved at the active DFB section. The η_{df} value is around 2.5 times higher than that reported in our previous work [48]. These improvements are considered to be caused by better matching between the DFB mode and the Bragg wavelength of the DBR section. Fig. 7 shows the power conversion efficiency of the membrane DR laser with a 61-μm-long DFB section. A maximum power conversion efficiency of 6.9% was obtained at a bias current of 1.2 mA. There is still room for improvement by the increase of internal quantum efficiency and the reduction of operation voltage.
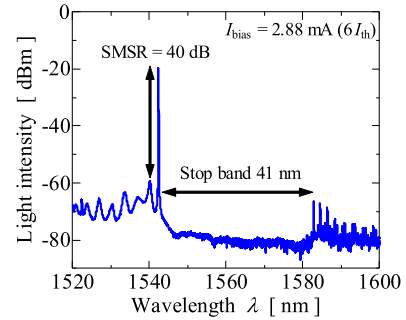
The lasing spectrum of this device at a bias current of 2.88 mA ($I_b = 6\,I_{th}$) is shown in Fig. 8. The single mode operation at lasing wavelength of 1542 nm with a side-mode suppression-ratio (SMSR) of 40 dB was obtained. A clear 41-nm-wide stop band was observed and used to estimate an index-coupling coefficient κ_i of $1840\,cm^{-1}$.

In this section, the membrane DR lasers with around 2.5 times higher DQE than that in previous report were shown, which may be attributed to the matching of the DFB lasing mode and the Bragg wavelength of the DBR section. The adoption of Au/Zn alloying for the p-side contact resulted in low bias voltage operation, which is important for low power consumption operation.
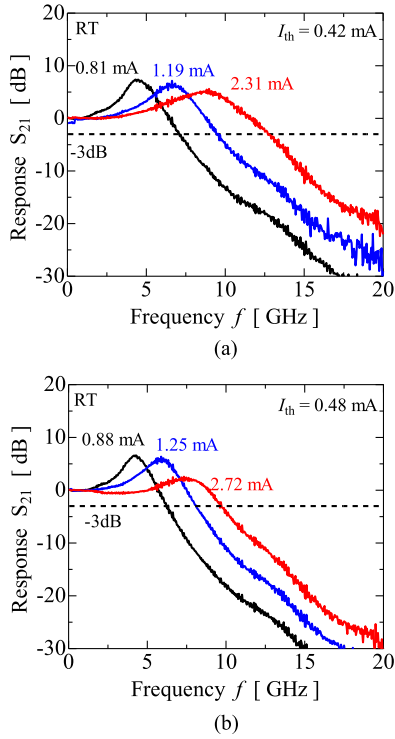
Fig. 9. Small signal response of membrane DR lasers with (a) 30-μm-long DFB section and 100-μm-long DBR section and (b) 61-μm-long DFB section and 50-μm-long DBR section.
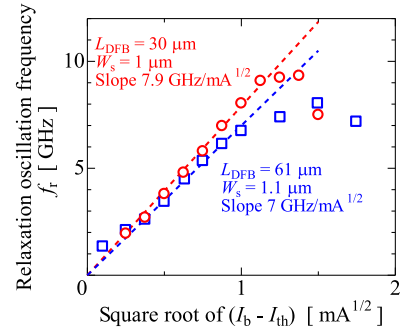

Fig. 10. Relaxation oscillation frequency f_r as a function of square root of $I_b - I_{th}$ for devices with DFB section lengths of 30 μm and 61 μm.
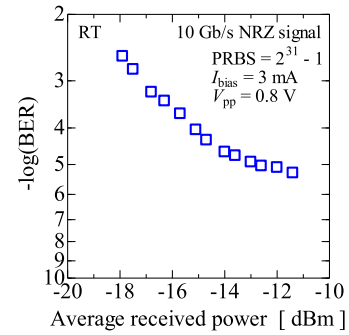

Fig. 11. Bit-error-rate as a function of average received power.

IV. DYNAMIC CHARACTERISTICS

In this section, direct modulation characteristics such as the small signal response and 10 Gbit/s large signal modulation characteristic of the membrane DR laser are given. First, the small signal measurement was performed using a vector network analyzer (VNA). A modulation signal was applied to the device using a 40-GHz-band high-speed signal-ground (SG) RF probe with 100 μm pitch. The light output from the front facet was coupled to a spherical-lensed single-mode fiber. The collected optical signal output was amplified by an erbium-doped fiber amplifier (EDFA), and then the amplified spontaneous emission (ASE) light was filtered by a tunable bandpass filter. The optical signal was finally detected by a 12 GHz PIN-photoreceiver.

Fig. 9 shows the small signal response S_{21} for the membrane DR lasers with DFB section lengths of 30 μm and 61 μm. It was confirmed that the relaxation oscillation frequency f_r and 3 dB bandwidth f_{3dB} increased with an increase of the bias current, and the maximum 3 dB bandwidth was 12.8 GHz at a bias current of 2.31 mA for the device with 30-μm-long DFB section and 9.7 GHz at a bias current of 2.72 mA for the device with 61-μm-long DFB section. These 3dB bandwidths are sufficient for 10 Gb/s operation.

Fig. 10 shows the relaxation oscillation frequency f_r as a function of the square root of bias current above the threshold for devices with DFB section lengths of 30 μm and 61 μm. Slope efficiencies of f_r (modulation current efficiency factor: MCEF) for the device with 30-μm-long DFB section and the device with 61-μm-long DFB section length were 7.9 GHz/mA$^{1/2}$ and 7 GHz/mA$^{1/2}$, respectively. These MCEF were much higher than the 3.0 GHz/mA$^{1/2}$ of conventional

(vertical current injection type) GaInAsP/InP DR lasers [56], thanks to the strong optical confinement effect as well as small active region of the membrane structure. The MCEF of the 30-μm-long device is higher than that of the 60-μm-long device due to the small active region. However, the value of 7.9 GHz/mA$^{1/2}$ for the 30-μm-long device was slightly smaller than the 11 GHz/mA$^{1/2}$ of the previously reported membrane DFB laser with the same active region volume of 0.9 μm^3 [43]. The reason for this is low differential gain due to the twice-higher threshold current density of 1.4 kA/cm^2 than that (700 A/cm^2) of the membrane DFB laser. To enhance this MCEF, low threshold current density operation is required by the introduction of a higher index-coupling coefficient structure.

Finally, large signal direct modulation was performed with the device with a 61-μm-long DFB section. For large signal direct modulation, the EDFA was not used. An electrical data signal with a pseudo-random bit sequence (PRBS) having a word length of $2^{31} - 1$ was generated by a pulse pattern generator. The output was monitored and attenuated before the photoreceiver. Fig. 11 shows the bit error rate (BER) as a function of the average received power of the 10 Gbit/s non return to zero (NRZ) signal. The bias current for the device and modulation voltage swing were set to 3 mA and 0.8 V_{pp}, respectively. A minimum BER of 5.4×10^{-6} was obtained. In order to investigate the reason for the high BER, a signal eye pattern was observed. Fig. 12 shows the eye pattern at an average received power of -11.4 dBm. The eye opening is unclear due to the noise. The reason for the noise is reflection back to the cavity due to the rear waveguide. An anti-reflection facet coating can improve this noise property. At this bias condition, the energy cost of the device is estimated to be 980 fJ/bit which is not close

TABLE I
SUMMARY OF STATE OF THE ART OF DFB/DR LASERS ON SI SUBSTRATE

Structure	Area [μm^2]	Threshold current [mA]	DQE [%/facet]	Max. output power [mW]	Modulation speed [Gb/s]	Energy cost [fJ/bit]	Institution
DFB*	800	8.8	~7	3.75	12.5	~11000	UCSB, USA [24]
DFB*	~1100	17	~15	6	40	~5000	U Ghent, Belgium [26]
DFB‡	73	0.9	~11	0.93	25.8	171	NTT, Japan [57]
DR†	40	0.6	~21	~0.65	25.8	132	NTT, Japan [50], [51]
DFB‡	30	0.21	5	~0.05	10	230	Tokyo Tech., Japan [43]
DR‡	67	0.48	26	0.36	10	980	Tokyo Tech., Japan (This work)

*The light output from active region was coupled to Si waveguide. †The light output from active region was coupled to InP waveguide. ‡The front facet was cleaved at active region.
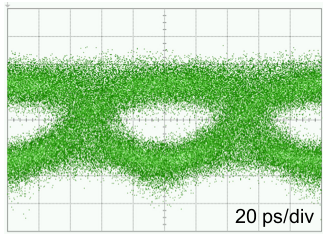

Fig. 12. Eye pattern of 10 Gbit/s NRZ signal with a $2^{31}-1$ pattern (inverted pattern).

to the required 100 fJ/bit. The reason for this is higher bias current compared with previous work [43] due to the noisy signal pattern.

The performances of DFB/DR lasers prepared on Si substrate are summarized in Table I. As mentioned in the introduction, DFB lasers coupled to Si waveguide have high energy cost in terms of application for on-chip optical interconnection. In contrast, the membrane lasers coupled to InP waveguide realized very low operating energy. In this study, the highest DQE was obtained by DR lasers (DFB laser integrated with DBR). Further reduction of operating energy can be expected by not only suppression of reflection but also reduction of threshold current as well as increase of DQE.

V. CONCLUSION

A membrane distributed-reflector (DR) laser with low threshold current and high efficiency operation was investigated as a promising light source for use in on-chip optical interconnections.

First, theoretical analysis of threshold current and external differential quantum efficiency of the membrane DR laser was carried out. The result shows that the DFB section length from 30 to 50 μm is suitable to obtain both low threshold current and high external differential quantum efficiency for the output power required from the minimum receivable power of a PIN-PD at 10 Gbit/s operation.

Next, membrane DBR laser and DR lasers were fabricated and evaluated. The membrane DBR laser with an active section length of 80 μm and DBR section length of 50 μm showed high external differential quantum efficiency of 35% at the front facet side, where the DBR reflectivity was estimated to be 75%. For the membrane DR laser with 61-μm-long DFB section and 50-μm-long DBR section, a threshold current of 0.48 mA, external differential quantum efficiency at the front waveguide side of 26%, and light output ratio of 13 were obtained. From the

lasing spectrum, single mode operation with an SMSR of 40 dB was obtained.

Finally, the modulation characteristics of membrane DR lasers were measured. In the small signal measurement, a modulation current efficiency factor (MCEF) of 7.9 GHz/mA$^{1/2}$ and 7 GHz/mA$^{1/2}$ for the devices with 30-μm-long DFB section and 61-μm-long DBR section were respectively obtained. Furthermore, BER of 5.4×10^{-6} was obtained. Although error-free operation was not obtained, the introduction of anti-reflection coating can improve the noise property. This shows the membrane DR laser can achieve high-speed modulation with low bias current due to the strong optical confinement effect in the thin semiconductor membrane structure.

These results show the membrane DR laser is a powerful candidate for on-chip light sources, in terms of low power consumption and high-speed data transmission. The operation energy can be improved by the introduction of a high-index-coupling coefficient structure with a small volume of the active region.

REFERENCES

[1] R. H. Dennard, F. H. Gaensslen, V. L. Rideout, E. Bassous, and A. R. LeBlanc, "Design of ion-implanted MOSFET's with very small physical dimensions," *IEEE J. Solid-State Circuits*, vol. 9, no. 5, pp. 256–268, Oct. 1974.

[2] P. Kapur, J. P. McVittie, and K. C. Saraswat, "Technology and reliability constrained future copper interconnects—Part I: Resistance modeling," *Trans. Electron Devices*, vol. 49, no. 4, pp. 590–597, Apr. 2002.

[3] P. Kapur, G. Chandra, J. P. McVittie, and K. C. Saraswat, "Technology and reliability constrained future copper interconnects—Part II: Performance implications," *Trans. Electron Devices*, vol. 49, no. 4, pp. 598–604, Apr. 2002.

[4] D. A. B. Miller, "Rationale and challenges for optical interconnects to electronic chips," *Proc. IEEE*, vol. 88, no. 6, pp. 728–749, Jun. 2000.

[5] G. Chen *et al.*, "Prediction of CMOS compatible on-chip optical interconnect," *Very Large Scale Integr. J.*, vol. 40, no. 4, pp. 434–446, Oct. 2006.

[6] K. Ohashi *et al.*, "On-chip optical interconnect," *Proc. IEEE*, vol. 97, no. 7, pp. 1186–1198, Jul. 2009.

[7] D. A. B. Miller, "Device requirements of optical interconnects to silicon chips," *Proc IEEE*, vol. 97, no. 7, pp. 1166–1185, Jul. 2009.

[8] P. Moser *et al.*, "81 fJ/bit energy-to-data ratio of 850 nm vertical-cavity surface emitting lasers for optical interconnects," *Appl. Phys. Lett.*, vol. 98, no. 23, pp. 231106-1–231106-3, Jun. 2011.

[9] S. Imai *et al.*, "Recorded low power dissipation in highly reliable 1060-nm VCSELs for 'Green' optical interconnection," *IEEE J. Sel. Topics Quantum Electron.*, vol. 17, no. 6, pp. 1614–1620, Nov. 2011.

[10] A. Kasukawa, "VCSEL technology for green optical interconnects," *IEEE Photon. J.*, vol. 4, no. 2, pp. 642–646, Apr. 2012.

[11] P. Moser, J. A. Lott, and D. Bimberg, "Energy efficiency of directly modulated oxide-confined high bit rate 850-nm VCSELs for optical interconnects," *IEEE J. Sel. Topics Quantum Electron.*, vol. 19, no. 4, Jul./Aug. 2013, Art. no. 1702212.

[12] M. Fujita, R. Ushigome, and T. Baba, "Continuous wave lasing in GaInAsP microdisk injection laser with threshold current of 40 μA," *Electron. Lett.*, vol. 36, no. 9, pp. 790–791, Apr. 2000.

[13] J. V. Campenhout *et al.*, "Electrically pumped InP-based microdisk lasers integrated with nanophotonic silicon-on-insulator waveguide circuit," *Opt. Express*, vol. 15, no. 11, pp. 6744–6749, May 2007.

[14] S. Matsuo *et al.*, "High-speed ultracompact buried heterostructure photonic-crystal laser with 13 fJ of energy consumed per bit transmitted," *Nature Photon.*, vol. 4, no. 9, pp. 648–654, Sep. 2010.

[15] B. Ellis *et al.*, "Ultralow-threshold electrically pumped quantum-dot photonic-crystal nanocavity laser," *Nature Photon.*, vol. 5, no. 5, pp. 297–300, May 2011.

[16] S. Matsuo *et al.*, "Room-temperature continuous-wave operation of lateral current injection wavelength-scale embedded active-region photonic-crystal laser," *Opt. Express*, vol. 20, no. 4, pp. 3773–9780, Feb. 2012.

[17] K. Takeda *et al.*, "Few-fJ/bit data transmissions using directly modulated lambda-scale embedded active region photonic-crystal lasers," *Nature Photon.*, vol. 7, no. 7, pp. 569–575, Jul. 2013.

[18] C.-T. Chen *et al.*, "Chip-level 1 × 2 optical interconnects using polymer vertical splitter on silicon substrate," *IEEE Photon. J.*, vol. 6, no. 2, Apr. 2014, Art. no. 7900410.

[19] T. Okamoto *et al.*, "Optically pumped membrane BH-DFB lasers for low-threshold and single-mode operation," *IEEE J. Sel. Topics Quantum Electron.*, vol. 9, no. 5, pp. 1361–1366, Sep./Oct. 2003.

[20] S. Sakamoto, T. Okamoto, T. Yamazaki, S. Tamura, and S. Arai, "Multiple-wavelengths membrane BH-DFB laser arrays," *IEEE J. Sel. Topics Quantum Electron.*, vol. 11, no. 5, pp. 1174–1179, Sep./Oct. 2005.

[21] S. Sakamoto *et al.*, "Strongly index-coupled membrane BH-DFB lasers with surface corrugation grating," *IEEE J. Sel. Topics Quantum Electron.*, vol. 13, no. 5, pp. 1135–1141, Sep./Oct. 2007.

[22] S. Arai, N. Nishiyama, T. Maruyama, and T. Okumura, "GaInAsP/InP membrane lasers for optical interconnects," *IEEE J. Sel. Topics Quantum Electron.*, vol. 17, no. 5, pp. 1381–1389, Sep./Oct. 2011.

[23] A. W. Fang *et al.*, "Electrically pumped hybrid AlGaAs-silicon evanescent laser," *Opt. Express*, vol. 14, no. 20, pp. 9203–9210, Oct. 2006.

[24] C. Zhang *et al.*, "Low threshold and high speed short cavity distributed feedback hybrid silicon lasers," *Opt. Express*, vol. 22, no. 9, pp. 10202–10209, May 2014.

[25] A. Abbasi *et al.*, "28 Gb/s direct modulation heterogeneously integrated C-band InP/SOI DFB laser," *Opt. Express*, vol. 23, no. 20, pp. 26479–26485, Oct. 2015.

[26] A. Abbasi *et al.*, "High speed modulation of a heterogeneously integrated InP/SOI DFB laser," *J. Lightw. Technol.*, vol. 34, no. 8, pp. 1683–1687, Apr. 2016.

[27] T. Okamoto, N. Nunoya, Y. Onodera, S. Tamura, and S. Arai, "Continuous wave operation of optically pumped membrane DFB laser," *Electron. Lett.*, vol. 37, no. 24, pp. 1455–1457, Nov. 2001.

[28] T. Maruyama *et al.*, "GaInAsP/InP membrane BH-DFB lasers directly bonded on SOI substrate," *Opt. Express*, vol. 14, no. 18, pp. 8184–8188, Sep. 2006.

[29] T. Okumura, T. Maruyama, M. Kanemaru, S. Sakamoto, and S. Arai, "Single-mode operation of GaInAsP/InP- membrane distributed feedback lasers bonded on Silicon-on-insulator substrate with rib-waveguide structure," *Jpn. J. Appl. Phys.*, vol. 46, no. 48, pp. 1206–1208, Dec. 2007.

[30] T. Okumura, T. Maruyama, H. Yonezawa, N. Nishiyama, and S. Arai, "Injection-type GaInAsP-InP-Si distributed-feedback laser directly bonded on silicon-on-insulator substrate," *IEEE Photon. Technol. Lett.*, vol. 21, no. 5, pp. 283–285, Mar. 2009.

[31] T. Okumura, H. Ito, D. Kondo, N. Nishiyama, and S. Arai, "Continuous wave operation of thin film lateral current injection lasers grown on semi-insulating InP substrates," *Jpn. J. Appl. Phys.*, vol. 49, no. 4, pp. 040205-1–040205-3, Apr. 2010.

[32] K. Oe, Y. Noguchi, and C. Caneau, "GaInAsP lateral current injection lasers on semi-insulating substrates," *IEEE Photon. Technol. Lett.*, vol. 6, no. 4, pp. 479–481, Apr. 1994.

[33] M. Futami *et al.*, "GaInAsP/InP lateral current injection laser with uniformly distributed quantum well structure," *IEEE Photon. Technol. Lett.*, vol. 24, no. 11, pp. 888–890, Jun. 2012.

[34] T. Shindo *et al.*, "GaInAsP/InP lateral-current-injection distributed feedback laser with a-Si surface grating," *Opt. Express*, vol. 19, no. 3, pp. 1884–1891, Jan. 2011.

[35] T. Shindo *et al.*, "Lateral-current-injection distributed feedback laser with surface grating structure," *IEEE J. Sel. Topics Quantum Electron.*, vol. 17, no. 5, pp. 1175–1182, Sep. 2011.

[36] T. Shindo, M. Futami, K. Doi, T. Amemiya, N. Nishiyama, and S. Arai, "Design of lateral-current-injection-type membrane distributed-feedback lasers for on-chip optical interconnections," *IEEE J. Sel. Topics Quantum Electron.*, vol. 19, no. 4, Jul./Aug. 2013, Art. no. 1502009.

[37] T. Shindo *et al.*, "Lateral-current-injection type membrane DFB laser with surface grating," *IEEE Photon. Technol. Lett.*, vol. 25, no. 13, pp. 1282–1285, Jul. 2013.

[38] D. Inoue *et al.*, "Room-temperature continuous-wave operation of GaInAsP/InP lateral-current-injection membrane laser bonded on Si substrate," *Appl. Phys. Express*, vol. 7, no. 7, Jun. 2014, Art. no. 072701.

[39] Y. Atsuji *et al.*, "Low-threshold-current operation of membrane distributed-feedback laser with surface grating bonded on Si substrate," *Jpn. J. Appl. Phys.*, vol. 54, no. 8, Jul. 2015, Art. no. 080301.

[40] D. Inoue *et al.*, "Sub-milliampere threshold operation of butt-jointed built-in membrane DFB laser bonded on Si substrate," *Opt. Express*, vol. 23, no. 6, pp. 7771–7778, Mar. 2015.

[41] D. Inoue *et al.*, "Monolithic integration of membrane-based butt-jointed built-in DFB lasers and p-i-n photodiodes bonded on Si substrate," *IEEE J. Sel. Topics Quantum Electron.*, vol. 21, no. 6, Nov./Dec. 2015, Art. no. 1502907.

[42] D. Inoue *et al.*, "High-modulation efficiency operation of GaInAsP/InP membrane distributed feedback laser on Si substrate," *Opt. Express*, vol. 23, no. 22, pp. 29024–29031, Oct. 2015.

[43] D. Inoue *et al.*, "Low-bias current 10 Gbit/s direct modulation of GaInAsP/InP membrane DFB laser on silicon," *Opt. Express*, vol. 24, no. 16, pp. 18571–18579, Aug. 2016.

[44] J.-I. Shim *et al.*, "Lasing characteristics of 1.5 μm GaInAsP-InP SCH-BIG-DR lasers," *IEEE J. Quantum. Electron.*, vol. 27, no. 6, pp. 1736–1745, Jun. 1991.

[45] K. Ohira, T. Murayama, S. Tamura, and S. Arai, "Low-threshold and high efficiency operation of distributed reflector lasers with width-modulated wirelike active region," *IEEE J. Sel. Topics Quantum Electron.*, vol. 11, no. 5, pp. 1162–1168, Sep./Oct. 2005.

[46] T. Shindo *et al.*, "Low-threshold and high-efficiency operation of distributed reflector laser with wirelike active regions," *IEEE Photon. Technol. Lett.*, vol. 21, no. 19, pp. 1414–1416, Oct. 2009.

[47] D. Takahashi *et al.*, "Carrier-transport-limited modulation bandwidth in distributed reflector lasers with wirelike active regions," *IEEE J. Quantum Electron.*, vol. 48, no. 5, pp. 688–695, May 2012.

[48] T. Hiratani *et al.*, "Room-temperature continuous-wave operation of membrane distributed-reflector laser," *Appl. Phys. Express*, vol. 8, no. 11, pp. 112701-1–112701-4, Oct. 2015.

[49] T. Hiratani *et al.*, "Energy cost analysis of membrane distributed-reflector lasers for on-chip optical interconnects," *IEEE J. Sel. Topics Quantum Electron.*, vol. 21, no. 6, pp. 299–308, Nov./Dec. 2015.

[50] H. Nishi *et al.*, "Membrane distributed-reflector laser integrated with SiOx-based spot-size converter on Si substrate," in *Proc. 2015 Eur. Conf. Opt. Commun.*, Sep. 2015, Paper WE.2.5.3.

[51] H. Nishi *et al.*, "Membrane distributed-reflector laser integrated with SiOx-based spot-size converter on Si substrate," *Opt. Express*, vol. 24, no. 16, pp. 18346–18352, Aug. 2016.

[52] K. Doi *et al.*, "Thermal analysis of lateral-current-injection membrane distributed feedback laser," *IEEE J. Quantum Electron.*, vol. 50, no. 5, pp. 321–326, May 2014.

[53] G. Björk and O. Nelsson, "A new exact and efficient numerical matrix theory of complicated laser structures: Properties of asymmetric phase-shifted DFB lasers," *J. Lightw. Technol.*, vol. LT-5, no. 1, pp. 140–146, Jan. 1987.

[54] D. Inoue *et al.*, "Butt-Joint Built-in (BJB) structure for membrane photonic integration," in *Proc. 25th Int. Conf. Indium Phosphide Related Mater.*, Kobe, Japan, May 2013, Paper TuD3-6.

[55] M. M. Raj, J. Wiedmann, Y. Saka, H. Yasumoto, and S. Arai, "1.5 μm wavelength DBR lasers consisting of 3λ/4-semiconductor and 3λ/4-groove buried with benzocyclobutene," *Electron. Lett.*, vol. 35, pp. 1335–1337, Aug. 1999.

[56] S. H. Lee *et al.*, "Low-power consumption high-eye-margin 10-Gb/s operation by GaInAsP/InP distributed reflector lasers with wirelike active regions," *IEEE Photon. Technol. Lett.*, vol. 23, no. 18, pp. 1349–1351, Sep. 2011.

[57] S. Matsuo *et al.*, "Directly modulated DFB laser on SiO2/Si substrate for datacenter networks," *J. Lightw. Technol.*, vol. 33, no. 6, pp. 1217–1222, Mar. 2015.

Takuo Hiratani (S'13) received the B.E. degree in electrical and electronic engineering from Kanazawa University, Ishikawa, Japan, in 2012 and the M.E. degree in 2014, in electrical and electronic engineering from the Tokyo Institute of Technology, Tokoyo, Japan, where he is currently working toward the Ph.D. degree in electrical and electronic engineering.

His research focuses on membrane-based photonic devices for on-chip optical interconnection.

Mr. Hiratani is a Student Member of the Institute of Electronics, Information and Communication Engineers and the Japan Society of Applied Physics.

Daisuke Inoue (S'16) received the B.E. and M.E. degrees in electrical and electronic engineering from Tokyo Institute of Technology, Tokyo, Japan, in 2013 and 2015, respectively, and he is currently working toward the Ph.D. degree in electrical and electronic engineering from Tokyo Institute of Technology.

His research focuses on membrane-based photonic devices for optical interconnection.

Mr. Inoue is a Student Member of the Institute of Electronics, Information and Communication Engineers, the Japan Society of Applied Physics, and the IEEE Photonics Society. He received the CSW2016 Best Student Paper Award.

Takahiro Tomiyasu received the B.E. degree in electrical and electronic engineering from Tokyo Institute of Technology, Tokyo, Japan, in 2015, and he is currently working toward the M.E. degree in the Department of Electrical and Electronic Engineering, Tokyo Institute of Technology.

His research focuses on membrane-based DFB lasers for optical interconnection.

Mr. Tomiyasu is a Student Member of the Institute of Electronics, Information, and Communication Engineers.

Kai Fukuda received the B.E. degree in electrical and electronic engineering from Tokyo Institute of Technology, Tokyo, Japan, in 2015, and he is currently working toward the M.E. degree in the Department of Electrical and Electronic Engineering, Tokyo Institute of Technology.

His research interest focuses on membrane-based DFB lasers for optical interconnection.

Mr. Fukuda is a Student Member of the Japan Society of Applied Physics.

Tomohiro Amemiya (S'06–M'09) received the B.S., M.S., and Ph.D. degrees in electronic engineering from the University of Tokyo, Bunkyō, Japan, in 2004, 2006, and 2009, respectively.

In 2009, he moved to the Quantum Electronics Research Center, Tokyo Institute of Technology as an Assistant Professor. Since 2016, he has been an Assistant Professor in the Institute of Innovative Research, Tokyo Institute of Technology, Meguro, Japan. His research interests include physics of photonic integrated circuits, metamaterials for optical frequencies, semiconductor light-controlling devices, and the technologies for fabricating these devices.

Dr. Amemiya is a member of the Optical Society of America, the American Physical Society, and the Japan Society of Applied Physics. He received the 2007 IEEE Photonics Society Annual Student Paper Award, the 2008 IEEE Photonics Society Graduate Student Fellowships, the 2012 Konica Minolta Imaging Award, the 2015 Yazaki Memorial Foundation Award, and the 2016 Young Scientists' Prize, the Commendation for Science and Technology by the Minister of Education, Culture, Sports, Science and Technology (MEXT).

Nobuhiko Nishiyama (M'01–SM'07) received the B.E., M.E., and Ph.D. degrees from the Tokyo Institute of Technology, Tokyo, Japan, in 1997, 1999, and 2001, respectively. During his Ph.D. degree, he demonstrated single-mode 0.98- and 1.1-μm VCSEL arrays with stable polarization using misoriented substrates for high-speed optical networks as well as MOCVD-grown GaInNAs VCSELs.

He joined Corning, Inc., New York, NY, USA, in 2001 and worked with the Semiconductor Technology Research Group. At Corning, he worked on several subjects, including short-wavelength lasers, 1060-nm DFB/DBR lasers, and long-wavelength InP-based VCSELs. Since 2006, he has been an Associate Professor in Tokyo Institute of Technology. His research interests include transistor lasers, silicon photonics, III–V silicon hybrid optical devices, and terahertz–optical signal conversions involving optics–electronics–radio integration circuits.

Dr. Nishiyama is a member of the Japan Society of Applied Physics, Institute of Electronics, Information and Communication Engineers (IEICE), and the IEEE Photonics Society. He received the Excellent Paper Award from the IEICE of Japan, in 2001, the Young Scientists' Prize in the Commendation for Science and Technology from the Minister of Education, Culture, Sports, Science and Technology in 2009, and the Ichimura Prize in Science for Distinguished Achievement in 2016.

Shigehisa Arai (M'83–SM'06–F'10) received the B.E., M.E., and D.E. degrees in electronics from Tokyo Institute of Technology, Meguro, Japan, in 1977, 1979, and 1982, respectively.

During his Ph.D. work, he demonstrated room-temperature CW operations of 1.11–1.67 μm long-wavelength lasers fabricated by liquid-phase epitaxy as well as their single-mode operations under rapid direct modulation. He joined the Department of Physical Electronics, Tokyo Institute of Technology, as a Research Associate in 1982, and joined AT&T Bell Laboratories, Holmdel, NJ, USA, as a Visiting Researcher from 1983 to 1984, on leave from the Tokyo Institute of Technology. Further, he became a Lecturer in 1984, an Associate Professor in 1987, and a Professor in the Research Center for Quantum Effect Electronics and the Department of Electrical and Electronic Engineering in 1994. Since 2004, he has been a Professor in the Quantum Nanoelectronics Research Center, Tokyo Institute of Technology.

His research interests include photonic integrated devices such as dynamic-single-mode and wavelength-tunable semiconductor lasers, semiconductor optical amplifiers, and optical switches/modulators. His research interests include studies of low-damage and cost-effective processing technologies of ultrafine structures for high-performance lasers and photonic integrated circuits on silicon platforms.

Dr. Arai is a member of the Optical Society of America, and a Fellow of the Institute of Electronics, Information and Communication Engineers (IEICE), and the Japan Society of Applied Physics (JSAP). He received the Excellent Paper Award from the IEICE of Japan in 1988, the Michael Lunn Memorial Award from the Indium Phosphide and Related Materials Conference in 2000, Prizes for Science and Technology in the Commendation for Science and Technology from the Minister of Education, Culture, Sports, Science and Technology in 2008, an Electronics Society Award and the Achievement Award from IEICE in 2008 and 2011, respectively, a JSAP Fellowship in 2008, and SSDM Award from the International Conference on Solid-State Devices and Materials in 2016.